α-particle nuclear surface absorption below the Coulomb barrier in heavy nuclei

M. Avrigeanu and V. Avrigeanu*

"Horia Hulubei" National Institute for Physics and Nuclear Engineering, Post Office Box MG-6, R-077125 Bucharest-Magurele, Romania

(Received 7 April 2010; revised manuscript received 3 May 2010; published 7 July 2010)

An analysis of all available α-particle-induced reaction cross sections on nuclei within the mass number range $121 \leqslant A \leqslant 197$, below the Coulomb barrier, is carried out. This analysis leads to an optical potential that describes the α-particle elastic scattering at low energies as well and both elastic-scattering and reaction data for $45 \leqslant A \leqslant 124$. The energy dependence of the surface imaginary potential depth is proved to be essential for understanding α-particle interaction behavior below the Coulomb barrier.

DOI: 10.1103/PhysRevC.82.014606 PACS number(s): 24.10.Ht, 24.60.Dr, 25.55.−e, 27.60.+j

I. INTRODUCTION

While the interactions of α particles with nuclei have been of special interest from the earliest days of nuclear physics, their unified description has been expected for two decades [1]. However, even today their reaction cross sections predicted below the Coulomb barrier can differ by one order of magnitude. This happens because the one-body complex optical potential that describes the combined effect of the Coulomb and nuclear field is still uncertain at these energies.

As a matter of fact, the widely used phenomenological optical model potential (OMP) parameters are mainly derived from the analysis of elastic-scattering angular distributions, which are ruled out below the Coulomb barrier B. The extrapolation to very low energies of global potentials from higher energies is not appropriate owing to the strong change in the number of open reaction channels close to the Coulomb barrier. This fact leads to a strong energy dependence of the OMP imaginary part [2], which takes into account all nonelastic interactions globally and accounts for the effect of removing flux from the elastic channel. Thus, an α-particle optical potential within this energy range can be validated only by analyzing reaction cross sections. However, because of their scarcity and small size owing to the Coulomb barrier penetration, the analysis of these reaction cross sections is challenging. Alternatively, besides its basic interest, an accurate account of the α-particle OMP is highly required by many nuclear astrophysics applications, as well as by the nuclear engineering design of fusion test facilities.

In fact, the present study complements a similar work carried out for target nuclei $45 \leqslant A \leqslant 124$ [2], and the OMP parameters given hereafter are suitable for the whole mass range. Both articles follow a former systematic study [3] that focused exclusively on the α-particle elastic scattering on nuclei in the mass region $A \sim 100$ and energies from ∼14 to 32 MeV. However, none of these works has addressed an eventual failure to describe reaction data and the related OMP features. Under these circumstances, we first considered a semimicroscopic OMP with a double-folding model (DFM) real part using an advanced version with the explicit treatment of the exchange component ([4] and Refs. therein). A semimicroscopic analysis of the experimental α-particle elastic scattering on $A \sim 100$ nuclei at energies below 32 MeV led to a suitable energy-dependent phenomenological OMP imaginary part that also used the dispersive correction to the microscopic DFM real potential. Second, a full phenomenological analysis of the same data provided a regional OMP parameter set [3,5] that can be used in further nuclear-reaction model calculations. Next, $A \sim 50$–120 nuclei and energies from ∼13 to 50 MeV were subjected to the same analysis, which also included an ultimate statistical-model (SM) assessment of available (α,γ), (α,n), and (α,p) reaction cross sections for target nuclei from ^{45}Sc to ^{118}Sn and incident energies below 12 MeV [2]. An additional analysis of (α,γ) and (α,n) reaction cross sections close to B, measured meanwhile for ^{92,94}Mo, ^{112}Sn, and ^{113}In [6,7] nuclei, reconfirmed this OMP appropriateness [8,9].

In the following we present a first analysis of the available α-particle-induced reaction cross sections on nuclei with the atomic mass number $121 \leqslant A \leqslant 197$, atomic number $Z \geqslant 51$, and around B, using an optical potential that describes also the α-particle elastic scattering. The extension of the previous OMP [2] to heavy nuclei is discussed in Sec. II along with the basis of the SM calculations involved in the present work. A further OMP amendment is described in Sec. III, emphasizing the role of (α,γ) reaction analysis for the understanding of the α-particle optical potential at the lowest energies. Conclusions are given in Sec. IV.

II. MODELS PARAMETERS AND ANALYSIS OUTLINE

A. OMP extension for heavy nuclei

The separation between the elastic-scattering above B and reaction cross-section analyses below B [2,3], where the OMP parameters resulting from the former are involved in the latter, have emphasized the OMP parameters responsible for the difficulties incurred in describing reaction data. As a result, the energy dependence of the diffuseness a_R of the real part of optical potential and the depth W_D of derivative-shape surface imaginary potential has to be modified for $E_{\mathrm{c.m.}}/B$ <0.9 to obtain an optical potential that describes equally well the low-energy α-particle-induced reactions and elastic scattering data. Additionally, it is necessary to determine if similar changes occur when the Coulomb barrier for heavier target nuclei increases.

*vavrig@ifin.nipne.ro

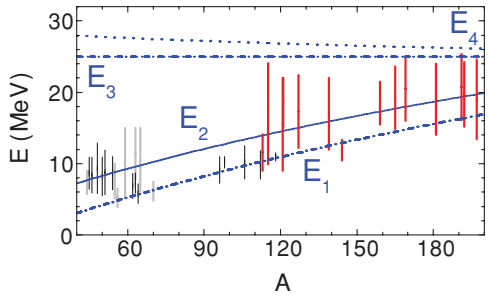

FIG. 1. (Color online) The A dependence of energies E_1 (dash-dotted) below which the depth W_D is constant, E_2 (solid) corresponding to $0.9B$, E_3 (dashed), and E_4 (dotted) given in Table I and the energy ranges (thick bars) of the (α,x) reaction data involved in this work for $A > 113$, as well as formerly analyzed (thin bars) and additionally checked in Ref. [2] for $A < 90$.

An extension of the semimicroscopic analysis that uses the DFM real potential for the whole mass region $50 < A < 209$ nuclei and energies from ∼8 to 50 MeV has also been carried out [10] with no DFM adjustable parameter or normalization. The analysis included the available α-particle elastic-scattering angular distributions for 13 target nuclei from ^{132}Ba until ^{209}Bi. The results of the same two-step OMP approach [3,8], shown in Figs. 1 and 2 of Ref. [10], actually endorse the previous regional parameter set. Minor changes were necessary only for the depth and diffuseness of the optical-potential real part, as given in Table I, with effects found to be larger only for $A \geqslant 132$.

Second, the aforementioned OMP parameters were used to carry out a first SM analysis of all available α-particle-induced reaction cross sections on 15 nuclei with $121 \leqslant A \leqslant 197$ [11]. One should note that the increased B values associated with medium nuclei move the energy range of interest close to ∼20 MeV (Fig. 1). Moreover, we have to limit our analysis to ∼25 MeV because of the pre-equilibrium emission effects that may trigger additional problems for the SM-calculated reaction cross sections. However, because of the scarcity of (α,γ) reaction data available with higher precision at these energies, which as a matter of fact exist only for ^{127}I, ^{144}Sm, and ^{197}Au, we first needed to take into account the most recent data for ^{113}In [7].

B. Statistical model input parameters

The experimental α-particle-induced or (n,α) reaction cross sections have not been previously taken into account [3] because of the problems associated with the remaining parameters needed in SM calculations [12]. For the same reason, we used a consistent set of local SM parameters established or validated on the basis of independent experimental information on, for example, neutron total cross sections, γ-ray strength functions based on neutron-capture data, and low-lying level and resonance data. Of particular interest for the present work

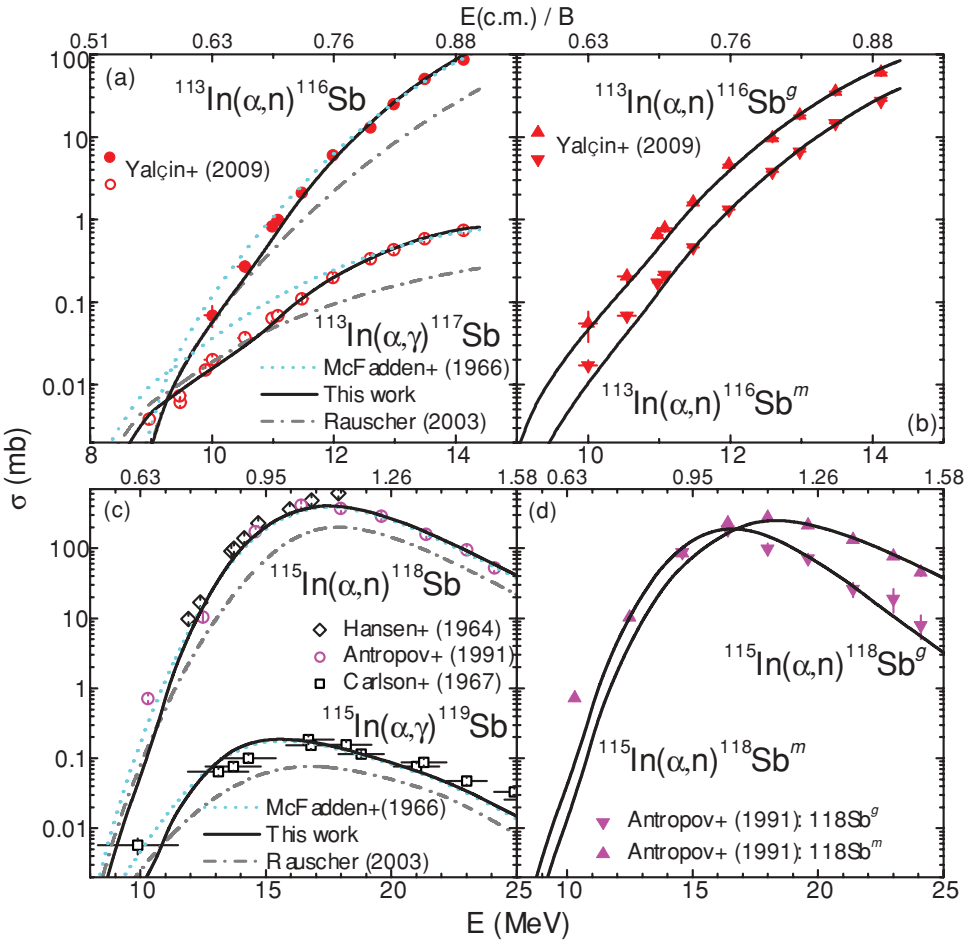

FIG. 2. (Color online) Comparison of measured [7,11] and (a,c) calculated (α,γ) and (α,n) reaction cross sections for the target nuclei ^{113,115}In nuclei, using the OMPs of Refs. [22] (dotted curves), [23] (dash-dotted), and Table I (solid). (b,d) The latter comparison for ^{113,115}In(α,n) reactions that produce the ground ^{116,118}Sb^g and isomeric ^{116,118}Sb^m states.

TABLE I. Optical potential parameters obtained by fit of the α-particle elastic-scattering and reaction cross sections on nuclei with $45 \leqslant A \leqslant 209$, at energies $E < 50$ MeV, in addition to the Coulomb potential of a uniformly charged sphere of reduced radius $r_C = 1.3$ fm. The energy-range limits[a] are in MeV. An asterisk used as superscript follows the parameters which were changed with respect to the optical potential of Ref. [2].

Potential depth (MeV)		Geometry parameters (fm)	
$V_R^* = 165 + 0.733Z/A^{1/3} - 2.64E,$	$E \leqslant E_3$	$r_R = 1.18 + 0.012E,$	$E \leqslant 25$
$= 116.5 + 0.337Z/A^{1/3} - 0.453E,$	$E > E_3$	$= 1.48,$	$E > 25$
		$a_R^* = 0.631 + 0.016Z/A^{1/3} - (0.001Z/A^{1/3})E_2,$	$E \leqslant E_2$
		$= 0.631 + 0.016Z/A^{1/3} - (0.001Z/A^{1/3})E,$	$E_2 < E \leqslant E_4$
		$= 0.684 - 0.016Z/A^{1/3} - (0.0026 - 0.00026Z/A^{1/3})E,$	$E > E_4$
$W_V = 2.73 - 2.88A^{1/3} + 1.11E$		$r_V = 1.34$	
		$a_V = 0.50$	
$W_D^* = 2.5 \pm 1.0$[b],	$E \leqslant E_1$	$r_D = 1.52$	
$= 22.2 + 4.57A^{1/3} - 7.446E_2 + 6E,$	$E_1 < E \leqslant E_2$	$a_D = 0.729 - 0.074A^{1/3}$	
$= 22.2 + 4.57A^{1/3} - 1.446E,$	$E > E_2$		

[a] $E_1^* = -3.28 - 0.762A^{1/3} + 1.24E_2$, $E_2 = (2.59 + 10.4/A)Z/(2.66 + 1.36A^{1/3})$, $E_3^* = 22.2 + 0.181Z/A^{1/3}$, $E_4^* = 29.1 - 0.22Z/A^{1/3}$.
[b] $W_D = 3.5$ for $A < 130$ while $W_D = 1.5$ fits better the data for $A > 130$.

has been the analysis of these data for all stable isotopes of, for example, Cd, Sn, and Te [13]. Actually, the systematical analysis of this neutron-capture data basis was carried out to obtain a suitable normalization of accurate γ-ray strength functions using independent experimental data within the same energy range as the (α,x) reaction cross sections which are the subject of this work.

The global and local OMPs of Koning and Delaroche [14] have usually been used for neutrons, while the γ-ray-transmission coefficients are obtained with a dominant electric dipole transition strength function $f_{E1}(\varepsilon_\gamma)$ given by the giant dipole resonance model with an energy-dependent Breit-Wigner (EDBW) line shape [15,16]. Moreover, we used the usual normalization procedure of f_{M1}, f_{E2}, . . . , relative to the dominant $E1$ contribution to calculate the radiative width $\Gamma_{\gamma 0}^{\mathrm{EDBW}}$ of the s-wave neutron resonances and to analyze thus the experimental average values $\Gamma_{\gamma 0}^{\mathrm{exp}}$ [17]. Next, systematic EDBW-model correction factors were established assuming that they are given by the ratio $F_{SR} = \Gamma_{\gamma 0}^{\mathrm{exp}} / \Gamma_{\gamma 0}^{\mathrm{EDBW}}$. It should be noted that the radiative width predicted for nuclei without resonance data are rather close to the results given by an interpolation formula proposed by Gardner and Dietrich [15] and available optionally within an updated version of SM code STAPRE-H95 [18] used in this work. Finally, the correctness of the adopted γ-ray strength functions has been proved by the consistency of the calculated and measured neutron-capture cross sections.

As far as the nuclear level density is concerned, the back-shifted Fermi gas (BSFG) formula was used for excitation energies below the neutron-separation energy, with the parameters a and Δ [19] obtained by a fit of the recent experimental low-lying discrete levels [20] and s-wave nucleon resonance spacings D_0 [17]. The smooth-curve method was adopted [21] for nuclei without resonance data, leading to a values of the even-even, odd-odd, and odd-mass nuclei that were next kept fixed during the fit of low-lying discrete levels.

Because consistent model calculations should concern the available data for all reaction channels and isotopes of an element, our analysis has included the earlier measured cross sections [11] for other isotopes of the same element, for example, the ^{113,115}In and ^{121,123}Sb, and various channels on the same target nucleus as (α,xn) on ^{121}Sb, with $x = 1, 2$ and (α,γ) and (α,n) on ^{139}La. The agreement of the calculated and accurately measured cross sections for the ground and isomeric states of ^{113,115}In [Figs. 2(b) and 2(d)] confirms the SM calculation accuracy and consistency.

C. Comparison of α-particle OMPs for heavy nuclei

The aim of the present analysis is twofold. Apart from setting up an optical potential that can accurately describe both the elastic-scattering and α-particle-induced reaction data, it also aims to understand the reasons why predictions of α-nucleus potentials [22,23] frequently used for heavier nuclei (e.g., Ref. [24]) are at variance with the measured reaction data. It is for this reason that we start this discussion by comparing the results obtained for ^{113,115}In (Fig. 2) using the OMP parameters of Refs. [22,23] and our own findings (Table I). We found that the present parameters provide a better data account at lowest energies in comparison with the well-known four-parameter global potential of McFadden and Satchler [22], while there is a similar description at energies closer to B. The OMP of Ref. [23], which has the same imaginary potential [22] but a lower real potential, leads to smaller reaction cross sections (Figs. 3–5), as usual for energies below the barrier [25–28].

III. THE OMP AMENDMENT FOR HEAVY NUCLEI

A. (α,γ) reactions

The (α,γ) reaction data for $A > 121$, below the Coulomb barrier, are available only for ^{127}I, ^{136}Xe, ^{139}La, ^{144}Sm, and ^{197}Au. Actually, the overall good agreement between the measured and calculated cross sections (Figs. 3–5) has confirmed the present α-particle OMP obtained by elastic-scattering data analysis within the whole range $45 \leqslant A \leqslant 197$ except for the lowest-energy-limit value of the surface imaginary

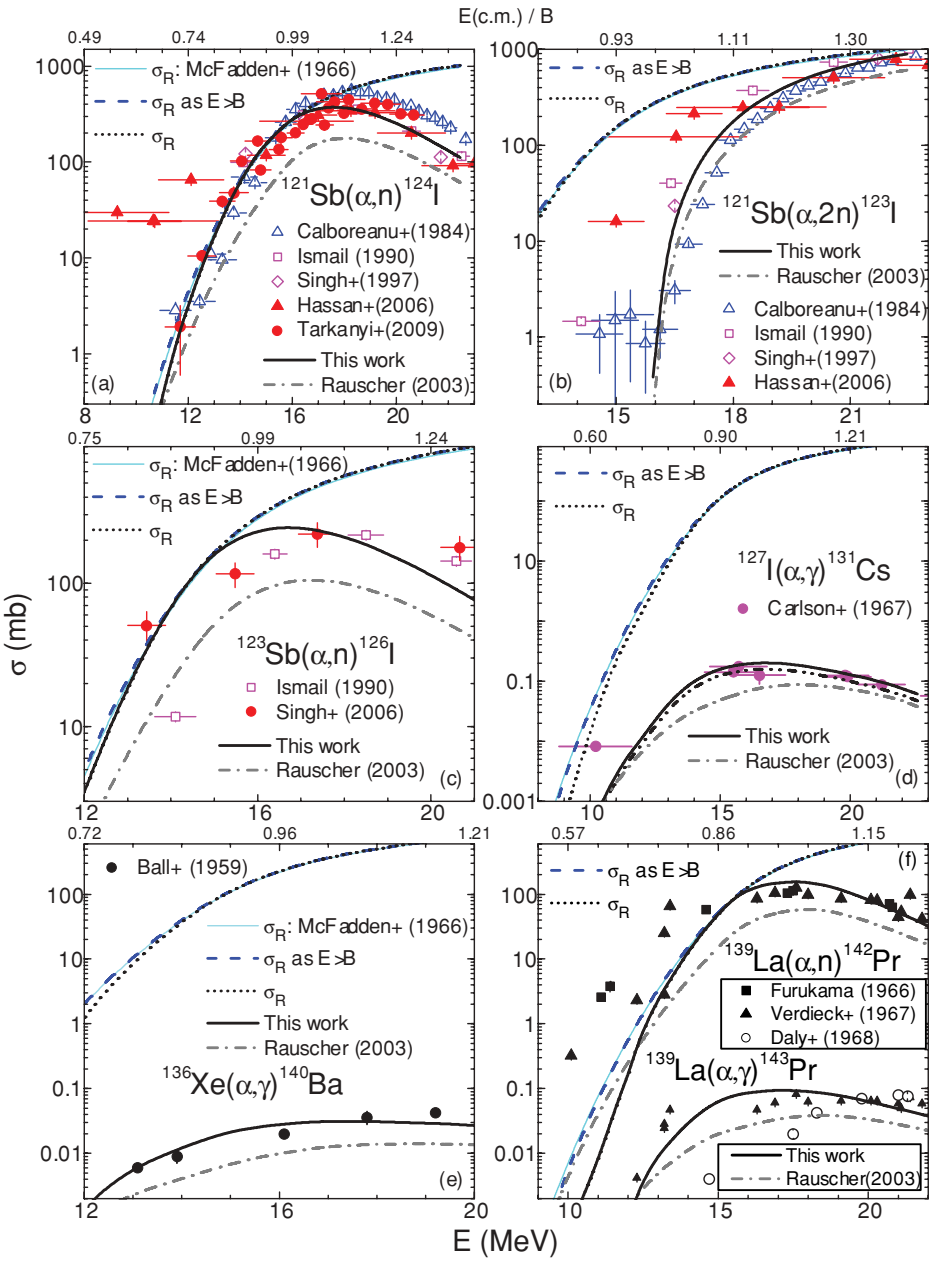

FIG. 3. (Color online) Comparison of calculated α-particle total reaction cross sections using the OMP parameters of Ref. [22] (thin solid curves), those obtained for energies above the energy limit E_2 (Table I) by elastic-scattering analysis alone (dashed), and their final values (dotted), as well as of the measured [11] and calculated cross sections of (α,x) reactions by using the OMP of this work (solid) and Rauscher [23] (dash-dotted) for the target nuclei ^{121,123}Sb, ^{127}I, ^{136}Xe, and ^{139}La. The dash-dot-dotted curve for the target nucleus ^{127}I (d) corresponds to the OMP of this work and a 20% decrease of the radiative width of s-wave neutron resonances used for normalization of the γ-ray strength function (see text).

potential depth W_D. It can be well established by means of the (α,γ) reaction study at α-particle energies where this reaction cross section stands actually for the α-particle total reaction cross section. The α-particle total reaction cross sections corresponding to the parameters given in Table I are shown in Figs. 3–5 and offer a straightforward view of a given reaction weight and its sensitivity to the α-particle OMP. Unfortunately, while there have been several $A < 120$ target nuclei (^{56}Fe, ^{58,62,64}Ni, ^{70}Ge, ^{96}Ru, ^{106}Cd, ^{112}Sn) with measured (α,γ) reaction data well described by the W_D value of $\sim$3.5 MeV [2], only the available data corresponding to the target nucleus ^{144}Sm are useful in this respect for $A > 130$. These data can be described by using a value $W_D \sim 1.5$ MeV as shown in Fig. 4(c). As a result, we adopt the value (2.5 ± 1.0) MeV for the lowest-energy limit of this parameters, as shown in Table I. Further experimental reaction cross sections should provide better parametrization constraint and make possible a physical insight of the corresponding trend.

A different case is that of the available (α,γ) reaction data for the other target nuclei ^{127}I, ^{136}Xe, ^{139}La, and ^{197}Au at α-particle energies where the (α,γ) reaction cross sections are at least two orders of magnitude smaller than the α-particle total reaction cross sections which go mainly in the (α,n) reaction channel. In this case the SM-calculated α-particle capture-reaction cross sections depend on the γ width as well. The results obtained for ^{127}I and ^{197}Au with $\sim$20% either decreased or increased s-wave neutron-resonance radiative widths used for normalization of the γ-ray strength functions are shown in Figs. 3(d) and 5(d), respectively. In this way we can evaluate the sensitivity of the calculated (α,γ) reaction cross sections to the adopted transmission coefficients for γ rays. As a matter of fact, these changes correspond to the differences between the

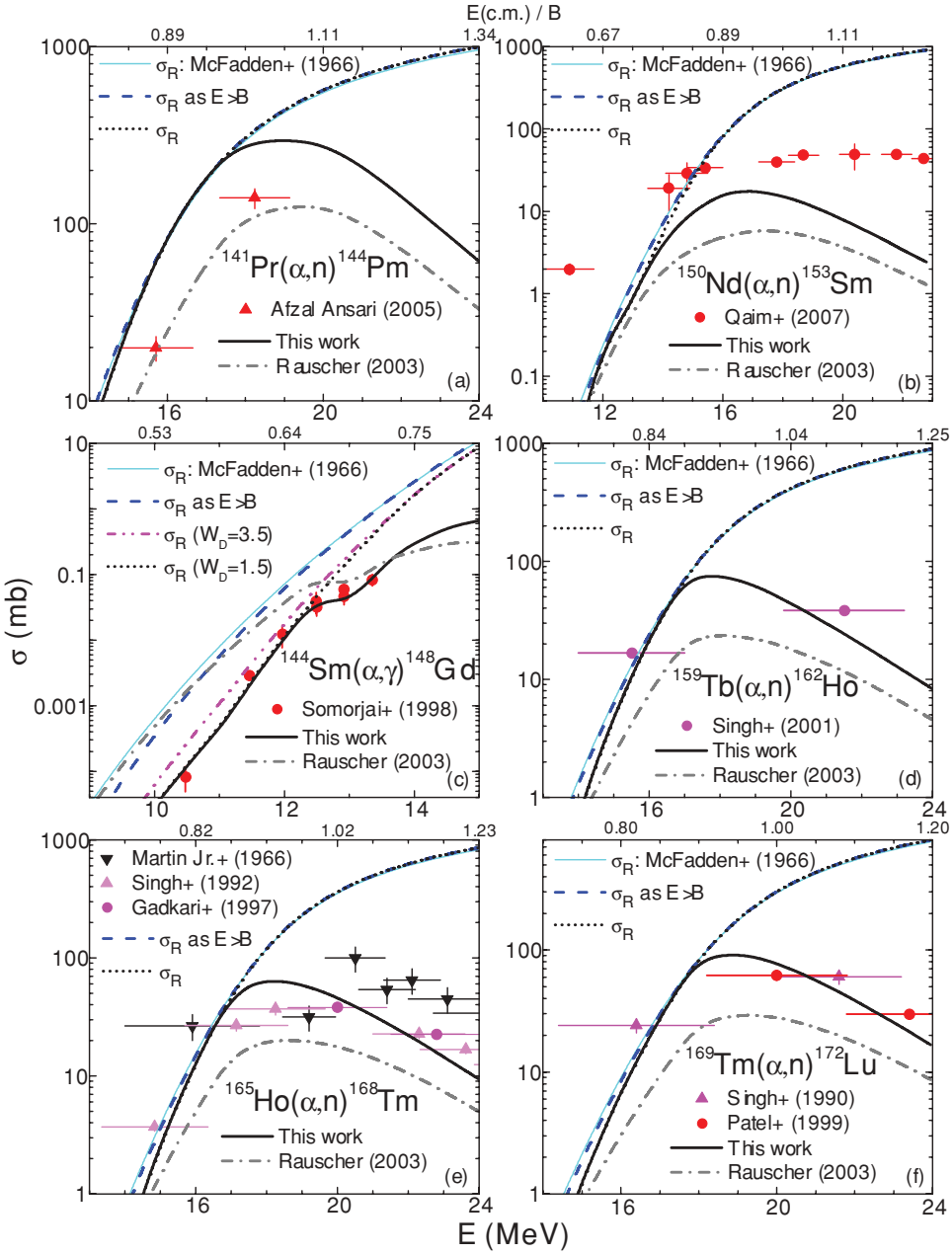

FIG. 4. (Color online) The same as in Fig. 3 but for the target nuclei ^{141}Pr, ^{150}Nd, ^{144}Sm, ^{159}Tb, ^{165}Ho, and ^{169}Tm.

radiative widths obtained through the normalization procedure mentioned in Sec. II B and the predictions of the interpolation formula in Gardner [15]. As a result, despite the quite larger sensitivity of the calculated (α,γ) reaction cross sections to the OMP parameters, the data for ^{127}I and ^{197}Au have only been used to check the adopted W_D value.

B. (α,xn) reactions

There are more data below the Coulomb barrier for the (α,xn) reaction than for the (α,γ) reaction, namely, for the target nuclei ^{121,123}Sn, ^{139}La, ^{141}Pr, ^{150}Nd, ^{159}Tb, ^{165}Ho, ^{169}Tm, ^{181}Ta, ^{192}Os, ^{191}Ir, and ^{197}Au. One may note the suitable description of these reaction cross sections within the critical energy range just above the threshold, which is usually a real challenge for SM calculations (e.g., in Figs. 4 and 8–9 of Ref. [7]). Some discrepancy could be seen just for a couple of target nuclei, ^{141}Pr and ^{150}Nd (Fig. 4). However, because there is currently only one data set for each of them, further measurements may be enlightening. Additional experimental data at the lowest energies will be especially helpful if an increased incident-energy accuracy is made available.

The α-particle total reaction cross sections corresponding to the parameters given in Table I are also shown in Figs. 3–5, which clearly emphasize a given reaction weight. The sensitivity of the calculated cross sections for such a particular reaction to the α-particle OMP is noticeable as well. Moreover, the total reaction cross sections corresponding to the four-parameter global potential of McFadden and Satchler [22] and the OMP parameter values obtained by the elastic scattering analysis for $E > E_2$ (Table I) are also included in these figures. It can therefore be seen that the larger overestimation of the

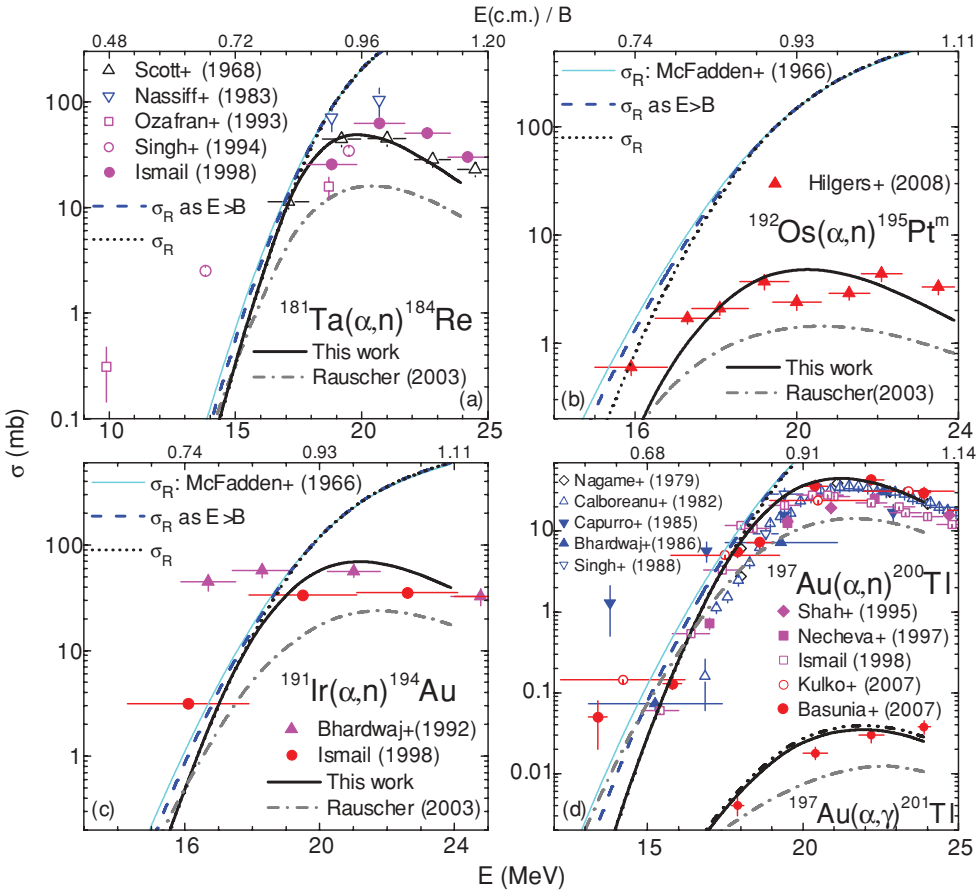

FIG. 5. (Color online) The same as in Fig. 3 but for the target nuclei ^{181}Ta, ^{192}Os, ^{191}Ir, and ^{197}Au, except the dash-dot-dotted curve for the target nucleus ^{197}Au (d), which corresponds to the OMP of this work and a 20% increase of the radiative width of s-wave neutron resonances used for normalization of the γ-ray strength function.

measured data by the extension to lower energies of the latter potential is the result of the extrapolation of the surface imaginary potential below the energy range where it was established. Actually, this OMP component increases with the energy increase, as more and more channels are thus opened. Furthermore, at higher energies the α-nucleus interactions take place to a greater extent inside the nucleus, owing to the volume part of the optical potential, while the surface component is decreasing and eventually vanishes. However, the elastic-scattering data analysis has been carried out at the energies above B, where the surface imaginary potential is already decreasing with the energy increase. Thus, while its estimation just above B is valuable as far as the understanding of the elastic-scattering is concerned, its extrapolation to much lower energies is unphysical and leads to larger disagreement between the calculated and measured data in comparison with a potential that has only a volume imaginary part. Nevertheless, the complementary reaction data analysis is the only method that permits an accurate estimation of the optical potential at the lowest α-particle incident energies.

IV. CONCLUSIONS

A correct estimation of the α-particle optical potential at energies below the Coulomb barrier is a key prerequisite for improved predictions of reaction data that are relevant at astrophysical energies as well as for α-particle emission leading to major radiation damage in fusion installations. Its understanding can be improved by comparing calculated and measured (α,x) reaction cross sections as long as they are quite close to the α-particle total reaction cross sections in the given energy range. A suitable surface-imaginary part of the optical potential proves to be essential in this respect, in comparison with adoption of a potential having only a volume imaginary part with a constant depth [22,23]. Moreover, the lowest energy limit of the surface imaginary potential depth W_D seems to have an essential importance for the accuracy of further cross-section predictions at these energies, eventually decreasing with the increase of the target nucleus mass. Nevertheless, additional measurements are needed to obtain a better parametrization constraint and to generate a physical insight into the corresponding trend.

To sum up, a larger overestimation of measured data may be generated through an extension to the lower energies of an optical potential that is established on the basis of only elastic-scattering data analysis and includes a surface imaginary part. This component increases first with the energy increase, as more and more reaction channels are opened, but then decreases and eventually vanishes as the larger-energy α-nucleus interactions take place to a greater extent

inside the nucleus. Because the elastic-scattering data analysis just above the Coulomb barrier facilitates the description of the latter side of the surface imaginary-potential energy dependence, the extrapolation to much lower energies of this partial trend becomes unphysical and leads to a larger breakdown than its absence. Nevertheless, the available data basis is still poor and further measurements with an increased incident-energy accuracy will be particularly helpful for a further understanding of the interactions of low-energy α particles.

ACKNOWLEDGMENTS

This work was partly supported by Fusion for Energy Grant No. F4E-2008-GRT-014 (ES-AC)-Action 1 and CNCSIS-UEFISCSU Project No. PNII-IDEI-149/2007.

[1] E. Gadioli and P. E. Hodgson, Rep. Prog. Phys. **52**, 247 (1989).
[2] M. Avrigeanu, A. C. Obreja, F. L. Roman, V. Avrigeanu, and W. von Oertzen, At. Data Nucl. Data Tables **95**, 501 (2009).
[3] M. Avrigeanu, W. von Oertzen, A. J. M. Plompen, and V. Avrigeanu, Nucl. Phys. A **723**, 104 (2003).
[4] Dao T. Khoa, Phys. Rev. C **63**, 034007 (2001).
[5] M. Avrigeanu, W. von Oertzen, and V. Avrigeanu, Nucl. Phys. A **764**, 246 (2006).
[6] W. Rapp, I. Dillmann, F. Käppeler, U. Giesen, H. Klein, T. Rauscher, D. Hentschel, and S. Hilpp, Phys. Rev. C **78**, 025804 (2008).
[7] C. Yalçin *et al.*, Phys. Rev. C **79**, 065801 (2009).
[8] M. Avrigeanu and V. Avrigeanu, Phys. Rev. C **79**, 027601 (2009).
[9] M. Avrigeanu and V. Avrigeanu, Phys. Rev. C **81**, 038801 (2010).
[10] M. Avrigeanu, W. von Oertzen, A. C. Obreja, F. L. Roman, and V. Avrigeanu, in *Proceedings of the 12th International Conference on Nuclear Reaction Mechanisms, 15–19 June 2009, Villa Monastero, Varenna, Italy*, edited by F. Cerutti and A. Ferrari (CERN, Geneva, 2010), CERN-Proceedings-2010-001-V-1.
[11] EXFOR Experimental Nuclear Reaction Data library [http://www.nndc.bnl.gov/exfor/].
[12] P. Demetriou, C. Grama, and S. Goriely, Nucl. Phys. A **707**, 253 (2002).
[13] V. Avrigeanu, F. L. Roman, and M. Avrigeanu, in *Proceedings of the 4th NEMEA-4 Workshop on Neutron Measurements, Evaluations and Applications, Prague, Czechia (2007)*, edited by A. Plompen (Institute for Reference Materials and Measurements, Geel, Belgium, 2008), European Commission Report EUR 23235 EN, p. 143.
[14] A. J. Koning and J. P. Delaroche, Nucl. Phys. A **713**, 231 (2003).
[15] D. G. Gardner and F. S. Dietrich, Report No. UCRL-82998, Lawrence Livermore National Laboratory, Livermore, CA, 1979.
[16] M. Avrigeanu, V. Avrigeanu, G. Căta, and M. Ivascu, Rom. J. Phys. **32**, 837 (1987).
[17] R. Capote *et al.*, Nucl. Data Sheets **110**, 3107 (2009).
[18] M. Avrigeanu and V. Avrigeanu, IPNE Report No. NP-86-1995, Bucharest, 1995, and Refs. therein; News NEA Data Bank **17**, 22 (1995).
[19] V. Avrigeanu, T. Glodariu, A. J. M. Plompen, and H. Weigmann, J. Nucl. Sci. Tech. Suppl. **2**, 746 (2002).
[20] Evaluated Nuclear Structure Data File (ENSDF), [www.nndc.bnl.gov/ensdf/].
[21] C. H. Johnson, Phys. Rev. C **16**, 2238 (1977).
[22] L. McFadden and G. R. Satchler, Nucl. Phys. A **84**, 177 (1966).
[23] T. Rauscher, Nucl. Phys. A **719**, 73c (2002); **725**, 295 (E) (2003).
[24] Gy. Gyürky, Z. Elekes, J. Farkas, Zs. Fülöp, G. G. Kiss, E. Somorjai, T. Szücs, R. T. Güray, N. Özkan, and T. Rauscher, J. Phys. Conf. Ser. **202**, 012004 (2010).
[25] A. R. Barnett and J. S. Lilley, Phys. Rev. C **9**, 2010 (1974).
[26] J. R. Huizenga and G. Igo, Nucl. Phys. **29**, 462 (1962).
[27] N. Takigawa and L. W. Put, Phys. Lett. B **84**, 371 (1979).
[28] P. E. Koehler, Yu. M. Gledenov, T. Rauscher, and C. Fröhlich, Phys. Rev. C **69**, 015803 (2004).